JBC Papers in Press. Published on February 27, 2019 as Manuscript RA118.006604
The latest version is at http://www.jbc.org/cgi/doi/10.1074/jbc.RA118.006604

Pyroglutamation of amyloid-βx-42 (Aβx-42) followed by Aβ1-40 deposition underlies plaque polymorphism in progressing Alzheimer's disease pathology

Wojciech Michno[1], Sofie Nyström[2], Patrick Wehrli[1], Tammaryn Lashley[3], Gunnar Brinkmalm[1], Laurent Guerard[1], Stina Syvänen[4], Dag Sehlin[4], Ibrahim Kaya[1], Dimitri Brinet[1], K. Peter R. Nilsson[2], Per Hammarström[2], Kaj Blennow[1,5], Henrik Zetterberg[1,3,5,6], and Jörg Hanrieder[1,3,6]**

From the [1]Department of Psychiatry and Neurochemistry, Sahlgrenska Academy at the University of Gothenburg, Mölndal, Sweden; [2]Department of Physics, Chemistry and Biology, Linköping University, Linköping, Sweden; [3]Department of Neurodegenerative Disease, UCL Queen Square Institute of Neurology, University College London, London, United Kingdom; [4]Department of Public Health and Caring Sciences, Uppsala University, Uppsala, Sweden; [5]Clinical Neurochemistry Laboratory, Sahlgrenska University Hospital, Mölndal, Sweden; [6]UK Dementia Research Institute at UCL, London, United Kingdom

Running Title: Molecular evolution of amyloid plaque polymorphism

***** To whom correspondence should be adressed: Jörg Hanrieder: Department of Psychiatry and Neurochemistry, Sahlgrenska Academy at the University of Gothenburg, Mölndal Hospital, House V, SE-43180 Mölndal, Sweden; jh@gu.se; Tel. +46 (31)3432377

Keywords: Alzheimer's disease, beta-amyloid, plaque polymorphism, hyperspectral imaging, imaging mass spectrometry, transgenic mice, neurodegeneration, pyroglutamation, pyroglutamic acid

ABSTRACT

Amyloid-β (Aβ) pathology in Alzheimer's disease (AD) is characterized by the formation of polymorphic deposits comprising diffuse and cored plaques. Since diffuse plaques are predominantly observed in cognitively unaffected, amyloid positive (CU-AP) individuals, pathogenic conversion into cored plaques appears to be critical to AD pathogenesis. Herein, we identified the distinct Aβ species associated with amyloid polymorphism in brain tissue from individuals with sporadic AD (s-AD) and CU-AP. To this end, we interrogated Aβ polymorphism with amyloid conformation–sensitive dyes and a novel in situ MS paradigm of hyperspectrally delineated plaque morphotypes. We found that maturation of diffuse into cored plaques correlated with increased Aβ1-40 deposition. Using spatial in situ delineation with imaging MS (IMS), we show that Aβ1-40 aggregates at the core structure of mature plaques, whereas Aβ1-42 localizes to diffuse amyloid aggregates. Moreover, we observed that diffuse plaques have increased pyroglutamated Aβx-42 levels in s-AD but not CU-AP, suggesting an AD pathology–related, hydrophobic functionalization of diffuse plaques facilitating Aβ1-40 deposition. Experiments in tgAPP$_{Swe}$ mice verified that similar to what has been observed in human brain pathology, diffuse deposits display higher levels of Aβ1-42 and that Aβ plaque maturation over time is associated with increases in Aβ1-40. Finally, we found that Aβ1-40 deposition is characteristic for cerebral amyloid angiopathy (CAA) deposition and maturation in both humans and mice. These results indicate that N-terminal Aβx-42 pyroglutamation and Aβ1-40 deposition are critical events in priming and maturation of pathogenic Aβ from diffuse into cored plaques, underlying neurotoxic plaque development in AD.

The conspicuous phenotypic variability of AD remains poorly understood, which makes it challenging to establish a common molecular basis of AD pathology. AD heterogeneity was previously linked to molecular and morphological traits of individual amyloid beta (Aβ) deposits (1,2). The formation of extracellular Aβ plaques has been identified as a major pathological hallmark of AD and a critical trigger of AD pathogenesis (3). According to the amyloid

cascade hypothesis, it was suggested that the phenotypic heterogeneity of AD pathology is induced by polymorphic Aβ fibrils that precipitates as heterogeneous plaque pathology, including (formation of) diffuse- and cored, mature plaques (4-8).

Morphologic heterogeneity of Aβ plaques has been linked to the structural- and chemical diversity of amyloid fibrils that consist of different Aβ peptide isoforms (9). These polymorphic fibrils are formed through structural transitions of different Aβ peptide isoforms during the aggregation process (1,2).

Plaque polymorphism, attributed to differing fibrillary components, has been shown to correspond to distinct spectral emission upon luminescent conjugated oligothiophene (LCO) based fluorescent amyloid staining (10-12). Specifically, plaque diversity as delineated by differential amyloid dye staining, was previously attributed to distinct amyloid traits prominent to different familial forms of AD, as well as in genetic mouse models of AD carrying the same mutations (13-15). On the histopathological level, this comprised varying patterns of both diffuse and cored Aβ plaque pathologies (16-19). Importantly, predominantly diffuse Aβ plaque pathology with almost no cored plaques, has also been identified in cognitively unaffected amyloid positive (CU-AP) individuals (20,21). This suggests that both the differing Aβ plaque morphotypes, but also molecular polymorphism at the Aβ fibril level and the associated Aβ peptide isoforms, are of importance for explaining the heterogeneity of AD pathology. While previous efforts have established that phenotypic heterogeneity of AD subtypes is reflected in morphological traits of individual plaque structures, associated biochemical characteristics including Aβ peptide pattern could not be delineated. We hypothesize that Aβ plaque polymorphism is associated with a plaque-specific Aβ peptide truncation pattern.

A major limitation in delineating amyloid pathology has been due the lack of imaging techniques to concomitantly acquire chemical and structural information of individual Aβ aggregates. To test our hypothesis, we therefore developed a multimodal chemical imaging paradigm for delineating plaque polymorphism and the associated Aβ peptide signatures in post-mortem human brain from sporadic AD (s-AD) and CU-AP individuals as well as in a transgenic AD mouse model ($tgAPP_{SWE}$) (22).

The results obtained here provide evidence for a relationship between Aβ peptide species ratio and Aβ plaque morphotypes (diffuse and cored), as indicated by conformational characteristics of Aβ plaques underlying peptide aggregates. Furthermore, as revealed by experiments in transgenic $tgAPP_{SWE}$ mice, such structural transition of the fibrils underlying Aβ plaques, likely reflects plaque maturation.

Results

Hyperspectral imaging delineates structural characteristics of amyloid plaque polymorphism

Structural polymorphism of Aβ plaque pathology can be delineated in an unbiased way by using novel, fluorescent amyloid probes based on luminescent conjugated oligothiophenes (LCO). These probes have different binding affinities to different amyloid structures as well as different electro-optic properties due to their flexible backbone allowing these molecules to adopt different backbone structures. Different LCOs can therefore be delineated using hyperspectral detection in fluorescent microscopy (23).

To understand how Aβ plaque polymorphism is related to distinct Aβ peptide content, we investigated structural and chemical characteristics of individual plaques in post-mortem human brain tissue from the temporal cortex of sporadic AD in the dementia stage and CU-AP cases (Table S1), as well as in transgenic AD mice ($tgAPP_{SWE}$).

To delineate spectral characteristics of Aβ polymorphism in human and mouse brain tissue, we used a double-stain strategy with two LCO based amyloid probes; tetra- and heptameric formyl-thiophene acetic acids (q- and h-FTAA) (Figure 1A, Figure S1A,B). This hyperspectral imaging paradigm was used for unbiased annotation of structurally distinct plaque morphotypes, i.e. cored and diffuse plaques (Figure S1B,C). The aim was then to characterize the corresponding Aβ peptide profile by isolating these plaques using laser microdissection with pressure catapulting (LMPC) followed by immunoprecipitation and mass spectrometric analysis (IP-MS, Figure S1C).

Using this chemical imaging paradigm, allowed us to annotate mature, Congo red (CR) positive, Aβ fibrils as well as immature fibrillary intermediates

of Aβ aggregation that are not detectable by thioflavin S (ThS) or congo red as previously described (Figure 1A, Figure S1B, Figure S2) (10). In the s-AD cases, we identified two major groups of Aβ plaque morphotypes: cored and diffuse, based on their morphology as well as their characteristic hyperspectral emission profiles that reflect differential LCO binding. Here, cored plaques exhibited a heterogenous emission profile with red emission at 540nm at the periphery, indicating h-FTAA binding, along with a characteristic blue-shift at the center region, corresponding to preferential q-FTAA binding (Figure 1A.I, A.II). In contrast, morphologically diffuse plaques in s-AD showed a homogeneous emission profile at 540nm across the entire plaque area, indicating h-FTAA binding (Figure 1A.III, A.IV) (10,11,13).

In contrast to s-AD pathology, brain tissue from CU-AP cases showed almost exclusively diffuse plaque morphotypes that exhibited emission profiles similar to the diffuse plaques observed in S-AD cases (Figure 1A.V, A.VI).

Given the spectral difference that we observed for the different plaque morphotypes, we sought to quantify differential LCO-binding in all plaques. For this, we calculated the mean emission ratio at 500nm/540nm, corresponding to the ratio of bound q-FTAA/h-FTAA (10). The results showed that q-FTAA staining in cored plaques was 14% higher than in diffuse plaques in s-AD and 25% higher than in diffuse plaques in CU-AP (Figure 1D).

Complementary, co-staining experiments of the LCOs with and Congo red as well as birefringence spectroscopy of CR show that q-FTAA-positive aggregates as observed in cored plaques are more fibrillar in structure as compared to h-FTAA-positive diffuse amyloid structures (Figure S2A).

Thus, our results suggest that diffuse plaques in s-AD and CU-AP are structurally similar and consist of immature, fibrillary Aβ aggregation inter-mediates, while cored plaques are characterized by formation of mature, q-FTAA- and CR positive-Aβ fibrils.

The Aβ1-40/Aβ1-42 ratio is associated with heterogenous plaque morphology

To characterize the Aβ composition pattern of these different plaque types, we isolated hyperspectrally annotated Aβ plaque-morphotypes using laser microdissection (Figure S1C.II). We extracted and selectively enriched Aβ species from the collected plaques, using a two step immunoprecipitation approach (Figure S1C.III). The individual Aβ species in the precipitate where then characterized using mass spectrometry (MS) (Figure S1C.IV) resulting in chemically specific MS peak data (Figure 1B,C) allowing for relative quantification of individual Aβ species in the plaque extracts (Figure 1E). Further, the detected mass signal were verified by high resolution MS and MS/MS (Figure S3-S5)

Our results showed that the Aβ1-40/Aβ1-42 ratio was 3.5-fold higher in cored plaques than in diffuse plaques in s-AD group (Figure 1B, C.I, E.I), and 7-fold higher than in the diffuse plaques found in the CU-AP group (Figure 1B, C.I, E.I). We observed a similar pattern for Aβ4-40 and Aβ4-42, the N-terminally truncated isoform of Aβ1-40 and Aβ1-42 (Figure S6A). Here, Aβ4-42 was the most dominant peak in the MS spectrum of all plaque types (Figure 1B). The Aβ4-40/Aβ4-42 ratio was 4-fold higher in cored plaques than in diffuse plaques in s-AD and 20-fold higher than in diffuse plaques present in CU-AP (Figure S6A). These results suggest that Aβ1-40 and Aβ4-40 are associated with formation of cored plaques and more mature Aβ fibrils in the heterogenous plaque pathology observed in AD dementia brains, while as mentioned previously, CU-AP brains contained almost exclusively diffuse plaques.

Given this pronounced increase of Aβ1-40 and Aβ4-40 in cored plaques, we investigated whether the relative amounts of these Aβ species correlated with the hyperspectral LCO signals. The results showed that Aβ1-40/Aβ1-42 correlated significantly with 500nm/540nm (R^2=0.43, $p<0.005$; Figure 1E.III). This indicates a positive association of Aβ1-40 with q-FTAA fluorescence and of Aβ1-42 with h-FTAA fluorescence. The correlation results for the ratio of the corresponding N-terminally truncated species, Aβ4-40/Aβ4-42, showed the same positive associations with 500nm/540nm (R^2=0.36, $p<0.01$; Figure S6B). This suggests that Aβx-40 species are associated with cored plaque areas while Aβx-42 peptides correlate with diffuse Aβ structures.

Pyroglutamate modification of Aβx-42 is increased in diffuse plaques in AD

While Aβ1-40 deposition was found to be the key parameter associated with cored plaques,

the results further show that the main chemical difference between diffuse plaques found in AD and CU-AP includes a significant increase in N-terminal pyroglutamate (pE) species of Aβ1-42 (AβpEx-42).

Our results showed that the AβpE3-42/Aβ1-42 ratio was two-fold higher in diffuse plaques in s-AD than in diffuse plaques in CU-AP, and three times higher in cored plaques in s-AD than in the diffuse plaques found in the CU-AP group (Figure 1C.II and E.II). We observed a similar pattern for AβpE11-42, where AβpE11-42/ Aβ1-42 ratio was two times higher in both cored and diffuse plaques in s-AD as compared to diffuse plaques present in CU-AP (Figure S7A.I). Similarly, to the Aβ1-40/Aβ1-42 ratio data, we asked whether the relative amounts of the AβpE species correlated with the hyperspectral LCO signals. The results showed that both AβpE3-42/Aβ1-42 (R^2=0.41, $p<0.005$; Figure 1E.IV) and AβpE11-42/Aβ1-42 (R^2=0.32, $p<0.01$; Figure S7A.II) correlated significantly with 500nm/540nm. These results suggest that pyroglutamate modification of Aβ1-42 in diffuse deposits is associated with Alzheimer specific Aβ pathology.

Amyloid beta 1-40 localizes to the center of cored plaques, while Aβx-42 species localize to diffuse aggregates

While the LMPC-IP based in situ MS method of hyperspectrally differentiated plaque morphotypes provided chemical signatures associated with Aβ polymorphism, no spatially resolved Aβ peptide identification data can be obtained on the single plaque level. We thus performed MALDI imaging mass spectrometry on s-AD and CU-AP tissue to resolve the localization of distinct Aβ peptides within single plaques and to delineate how this correlates with LCO staining (Figure 2A). Here, we observed that the Aβ1-40 signal was primarily localized to the center of the cored plaques in s-AD brain tissue but was not detected in diffuse plaques in s-AD and CU-AP as visualized in the single ion images (Figure 2 AI-III). In contrast, Aβ1-42 distributed to the periphery of cored plaques (Figure 2A.IV, A.VII). Further, Aβ1-42 was strongly localized to diffuse plaques in both s-AD (Figure 2A.V, A.VIII) and CU-AP (Figure 2 A.VI, A.IX). These results are well in line with our LMPC-IP-MS data (Figure 1), and further verify that indeed Aβ1-40 (and Aβ4-40; Figure S6C) is associated with mature Aβ fibrils and q-FTAA staining, respectively; while Aβ1-42 (and the more dominant Aβ4-42 signal (Figure S6D)) is associated with diffuse, mono-filamentous, protofibrillar Aβ assemblies that are found in diffuse plaques both in s-AD and CU-AP. Further, in line with the full length Aβ1-42, the corresponding pE species, AβpE3-42 and AβpE11-42 showed localization to diffuse areas of cored plaques (Figure 2B.I and Figure S7C.I) as well as diffuse plaques in s-AD, (Figure 2B.II, and Figure S7C.II) and CU-AP (Figure 2B.III and Figure S7C.III).

Chemical Characteristics of Amyloid Plaque Polymorphism in Humans Are Equivalent to tgAPP$_{SWE}$ Mouse Model

Our hyperspectral imaging results obtained for plaque morphotypes in s-AD and CU-AP are in line with previous observations in transgenic models with Aβ pathology (10,23,24). To determine whether core and diffuse plaque specific spectral properties are reflected in a general shift in Aβ peptide ratio, we performed LMPC and IP-MS on LCO delineated plaque morphotypes in 12- and 18-month-old tgAPP$_{SWE}$ mice that display heterogenous plaque pathology, including cored, diffuse plaques and cerebral amyloid angiopathy (CAA) (Figure 3A) (25).

In 12-month-old mice, we observed deposition of small compact plaques that primarily localized to the cortex, while almost no plaque formation was observed in the hippocampus (Figure 3A, B.I). This is in line with previous findings in different transgenic mouse models carrying the Swedish double mutation of APP. In these studies, an initial formation of smaller cored Aβ deposits at 10-12 months is reported, that is followed by rapid and exponential growth of both cored, as well as few diffuse- plaques, until, full-blown plaque pathology is reached at 18 months (25-27). Our double LCO staining results obtained from 12-month-old mice showed that these early Aβ plaques displayed a pronounced core structure (Figure 3B.II). The emission profile across the center of these early small, compact plaques showed however a more heterogenous blue shift (Figure 3B.III), as compared to the spectral data observed for cored plaques in s-AD.

In 18-month-old mice, we observed Aβ plaque pathology with heterogeneous morphology and

LCO annotated-optical properties in both the cortex and hippocampus. Here, we detected two major subpopulations of plaque morphotypes in both cortex and hippocampus including cored plaques and diffuse plaques as observed for s-AD (Figure 3B.IV-VII). At this age, the majority of plaques did exhibit a congo-red positive, core structure observed in brightfield and birefringence microscopy (Figure S2B-C, (25)) that displayed pronounced q-FTAA staining in the center (Figure 3B.IV, B.V). In contrast, diffuse plaques showed a homogenous emission profile at 540 nm across the plaque area, corresponding to h-FTAA (Figure 3B.VI, B.VII). Further, the emission wavelength ratio: 500nm/540nm (q-FTAA/h-FTAA) (10) was 60% higher in cored deposits as compared to diffuse in both the cortex and hippocampus. (Figure 3C).

We then determined the Aβ peptide profiles of all plaque types in all mice at both ages using laser microdissection and IP-MS for relative quantification of the individual Aβ species based on their MS traces (Figure 3D). Our results showed that there was no difference in Aβ1-40/Aβ1-42 ratio in between cored plaques in 12-month-old mice and diffuse plaques in 18-month-old mice (Figure 3E.I), In contrast, the Aβ1-40/Aβ1-42 ratio in cored plaques in older mice was two times higher than in cored plaques in 12-month-old mice (Figure 3E.I).

In 18-month-old animals, the Aβ1-40/Aβ1-42 ratio in cored plaques was also two times higher as compared to diffuse plaques, which was consistent in both the cortex and the hippocampus (Figure 3D, 3E.II). Similar to the human data, we found that the spectral emission ratio of the 500nm/540nm correlated significantly with Aβ1-40/Aβ1-42 peptide ratio in both cortex (Figure 3F.I; R^2=0.64, $p<0.005$) and hippocampus (Figure 3F.II; R^2=0.82, $p<0.005$). This indicates that, in accordance with plaque characteristics observed in human Aβ pathology, q-FTAA binding correlates with Aβ1-40 and that Aβ1-40 is associated with formation of cored plaques.

In order to confirm the localization of Aβ1-40 to cored plaque structures, we further verified these results for LCO outlined plaques using MALDI imaging MS on adjacent tissue slides (Figure 4A, B). The results showed localization of Aβ1-40 to core structures for small cored plaques in 12-month-old mice, while Aβ1-42, displayed a more heterogenous localization as illustrated in the individual ion images (Figure 4 A.I-III).

For 18-month-old $tgAPP_{SWE}$ mice, our MALDI IMS experiments showed peptide localization patterns similar to the findings observed in human tissue. Here, Aβ1-40 localized pre-dominantly to the central core structures of cored deposits (Figure 4B.I), In contrast, Aβ1-42 localized primarily to diffuse plaques and diffuse peripheral structures of cored deposits (Figure 4B.II, B.III).

This suggested that the LCO spectral pattern and the associated increase in Aβ1-40/Aβ1-42 peptide ratios are comparable between cored plaques observed in human AD as well as transgenic mouse model of AD. Moreover, these results show an age-associated change of spectral characteristics towards q-FTAA emission at 500nm along with an increase in Aβ1-40/Aβ1-42 ratio. Overall, this suggests that plaque maturation associated with AD pathogenesis is associated with conformational rearrangement from diffuse to cored deposits (10), and an interplay of Aβ1-40 and Aβ1-42 during incorporation into maturing fibrils (28).

Cerebral amyloid angiopathy (CAA) follows age-associated patterns observed for cored plaque

CAA is another characteristic in AD amyloid pathology and is suggested to be associated with the presence of cored amyloid deposits (29). Similarly, CAA is observed in both 12- and 18-month-old transgenic mice harboring the Swedish APP mutation (30-32). To investigate a chemical link between plaque polymorphism and vascular amyloidosis, we examined the LCO spectral characteristics and the Aβ peptide signature of CAA in human s-AD and $tgAPP_{SWE}$ mice.

Our results showed that CAA in s-AD patients showed a strong q-FTAA positive blue emission across the vessel wall of individual CAA deposits (Figure 5A.I, II). IP-MS of laser micro dissected CAA from s-AD tissue showed a dominant signal for Aβ1-40 and Aβ4-40, while no Aβ 1-42 was detected (data not shown). This was verified with MALDI IMS of individual CAA in human s-AD brain tissue, where Aβ1-40 was found to localize within the CAA deposits (Figure 5B.I). In contrast, no Aβ1-42 was found to localize within CAA deposits (Figure 5B.II, III).

In transgenic mice, CAA formation was observed in the cortex of 12-month-old mice and in the

cortex and hippocampus in older animals at 18 months (Figure 5A.III-VI). Spectral analysis of LCO stained brain tissue showed different cross-sectional emission profiles with increasing age. In 12-month-old mice, vascular amyloid deposits showed strong h-FTAA emission across their surface area (Figure 5A.III, IV). In 18-month-old mice, we observed a blue shift at the center of the vessel wall in these CAA structures, indicating a more mature Aβ aggregation state (Figure 5A.V, VI), IP-MS of laser-micro dissected CAA from transgenic mice showed that the Aβ1-40/Aβ1-42 ratio was five times increased in CAA in 18-month-old animals as compared to CAA in 12-month-old mice (Figure 5C).

To further verify the change in Aβ1-40/Aβ1-42 ratio, we performed MALDI IMS analysis on CAA in $tgAPP_{SWE}$ mouse brain. For 12-month-old mice, our IMS results show that both Aβ1-40 (Figure 5B.IV) and Aβ1-42 (Figure 5B.V) localize to CAA pathology (Figure 5B.VI). In 18-month-old mice, we observed a strong localization of Aβ1-40 to CAA (Figure 5B.VII), while the signal for Aβ1-42 showed only a weak localization to CAA (Figure 5B.VIII, B.IX). Taken together the data obtained for plaque pathology in transgenic mice suggest that increased Aβx-40 deposition playa a crucial role in maturation of both vascular amyloidosis and extracellular amyloid plaques and core formation, respectively.

Discussion

In this study, we investigated whether structural polymorphism of Aβ plaque morphotypes is associated with distinct Aβ chemistry. Our results show that cored plaques in s-AD are characterized by deposition of Aβ1-40, whereas diffuse plaques in both s-AD and CU-AP are characterized by deposition of Aβ1-42. Further, our data show that diffuse plaques in s-AD show increased levels of pyroglutamate-modified N-terminally truncated Aβ1-42 species (N-pyro-E Aβ; AβpE3-42, AβpE11-42) as compared to diffuse plaques in CU-AP. Imaging mass spectrometry identified Aβ1-40 localization in the center of cored plaques, suggesting that Aβ1-40 is associated with mature amyloid structures and dense fibrils, respectively, within cored plaques in s-AD. In contrast, diffuse areas of cored deposits, as well as diffuse plaques in both s-AD and CU-AP were largely composed of Aβ1-42. The corresponding pyro-E peptides AβpE3-42 and AβpE11-42 localized to diffuse structures as well. Since plaques in CU-AP show primarily diffuse morphology, these results suggest that full length Aβ1-42, while being indicative of general amyloidosis, is not the primary neurochemical trait associated with Aβ pathogenicity and toxicity in AD.

These findings appear to stand in contrast to the current perception that Aβ1-42 is the most relevant Aβ species associated with AD pathogenesis as suggested by CSF biomarker findings, where decreased Aβ1-42 levels, but not Aβ1-40, point toward brain wide accumulation of Aβ1-42 (33-35).

Plaque pathology in CU-AP with diffuse Aβ deposits could therefore represent prodromal AD pathology that given enough time would progress towards formation of mature, cored amyloid plaques as observed here, and also previously reported for $tgAPP_{SWE}$ (23) as well as APP23 and APP/PS1 mice (10). Our data on both human and mice samples suggest that this maturation and core formation involves deposition of Aβ 1-40 at the core.

Indeed, previous investigations on in situ Aβ quantification showed 20-fold higher levels of fibrillar Aβ1-40 and only 2-fold higher Aβ1-42 levels in brain tissue from AD patients, as compared to CU-AP patients (36,37). Further, in IHC based studies, Aβ1-40 was suggested to be associated with cored plaque formation in s-AD along with predominant Aβ1-42 staining of diffuse plaques both in AD and CU-AP (38). While pronounced CAA formation, characterized by predominant deposition of Aβ 1-40 was shown to result in decreased CSF levels of Aβ1-40 in patients with severe CAA (39), no such results have been reported for AD associated Aβ plaque pathology.

One could therefore speculate that the effect of this plaque specific Aβ 1-40 deposition is difficult to detect in CSF. Presumably, this is due to the general high abundance of Aβ1-40 in the brain, where the change in equilibrium of deposited and soluble Aβ1-40 as a consequence of plaque maturation (and Aβ1-40 deposition) is too minor to be reflected in the periphery.

An increase of Aβ1-42 in the brain, as indicated by decreased CSF levels, point to a general increased plaque load irrespective of plaque morphology and

can be explained by that Aβ1-42 is spherically accumulated in all plaques, including cored plaques, and thereby accounts for a significantly larger part of the plaque volume. Indeed, by comparing relative values, an increase in Aβ1-40/Aβ1-42 ratio seems to originate from increased Aβ1-40. Since Aβ1-40 is confined to the core structures that are smaller in volume relative to the total plaque volume, the amount may be underestimated by histological, antibody-based staining techniques. This is also consistent with western blot-based results reported on laser-microdissected plaques in s-AD, CU-AP and tgAPP/PS2 mice, which showed that cored and diffuse plaques were found to contain predominantly Aβ1-42; while the Aβ1-40/Aβ1-42 ratio was higher in cored plaques as compared to diffuse plaques owing to a higher content of Aβ1-40 (40).

In line with this, our observation in $tgAPP_{SWE}$ mice show an increased q-FTAA staining pattern and Aβ1-40/Aβ1-42 ratio in cored plaques compared to diffuse plaques, which was demonstrated with LCO/LMPC and IP-MS, as well as imaging MS. These data are supported by previous, immunohistochemistry (IHC)-based studies on plaque polymorphism in transgenic mice, that demonstrated a prominent Aβx-40 immunoreactivity within plaque cores, while Aβx-42 was found to stain mostly the radial periphery of cored plaques as well as diffuse deposits (25,27,38,41). The chemical and spectroscopic properties of diffuse parts of cored plaques as well as diffuse plaques in s-AD and diffuse plaques in CU-AP were consistent with respect to h-FTAA emission and Aβ1-42 content.

Given previous data on LCO delineated plaque maturation in transgenic mice (10) and cross seeded amyloidosis (42) and the here identified Aβ correlates, this suggests that diffuse plaques are precursors of cored plaques and that this maturation is associated with AD pathogenesis. This plaque maturation process is characterized by increased q-FTAA binding and the corresponding chemical correlate is Aβ1-40 that accumulates within the core region of mature plaques upon nucleation.

This is further supported by our results from $tgAPP_{SWE}$ mice, where we followed Aβ plaque pathology over time. While the general sample size was not large, these data showed clear trends and statistically significant changes in chemical plaque pathology that were tantamount to the findings in human tissue. In detail, early compact plaques observed in 12-month-old mice show higher relative amounts of Aβ1-42 and h-FTAA staining as compared to cored plaques in 18-month-old animals. Chemically, the early compact plaques at 12 months were similar to diffuse plaques observed in older mice that also contain relatively higher amounts of Aβ1-42 as compared to cored plaques. This suggests again that an increase in Aβ1-40/Aβ1-42 ratio is associated with plaque maturation of diffuse plaques into cored plaques via recruitment and deposition of Aβ1-40. Based on our observations, a possible pathological mechanism of plaque formation suggests initial seeding of extracellular Aβ aggregation through accumulation of soluble Aβ1-42 that is predominantly secreted during rising amyloid (43). This is followed by nucleation and maturation upon recruitment of Aβ1-40, which is in line with previous observations in $tgAPP_{SWE}$ mice (44).

Along that line, a prominent role of Aβ1-42 for initial plaque deposition has been suggested previously based on data in human AD brain (26) and transgenic mice (16) as well as for seeded Aβ-pathology in different transgenic mice, including tgAPP/PS1 and tgAPP23 (42). Aβ1-42 has been shown to rapidly form oligomers and subsequently fibrils, as compared to other C-terminally truncated Aβ species (45). In contrast, independent mechanisms for cored plaque formation have been suggested based on experiments in different transgenics, where cored plaques are also observed in younger mice ((31,46,47). This in line with our observations for younger mice, where only small compact/cored plaques where observed. However, it is still under debate whether this is a consequence of massive APP overexpression and Aβ production leading to rapid plaque formation and nucleation in neocortical areas, which might not be representative for how Aβ pathology is initiated in human AD.

Together with the data on C-terminal Aβ species, our observations on increased pyroglutamate-modified N-terminally truncated Aβ42 (N-pyro-E Aβ; AβpE3-42, AβpE11-42) in diffuse plaques in AD but not in CU-AP further suggest a prominent role of Aβ1-42 functionalization in seeding Aβ pathology in AD. Indeed, N-pyro-E-Aβ42 truncation has previously been identified to be

prominent in brain extracts (37) and senile plaques in AD following initial Aβ1-42 aggregation (38,48). Interestingly, AβpE3-42 has been suggested to be the dominating Aβ species in senile and diffuse plaques in AD, downs syndrome (DS) and CU-AP (38,49,50). In contrast, our data clearly show that the dominating species in all plaques is Aβ4-42 and that this truncation is not differing in between plaque types and disease state and is therefore rather an unspecific metabolite of Aβ1-42. One explanation for this discrepancy is that all previous data were based on detection in situ or in brain extracts using an antibody towards Aβ pE3-42 that could be cross-reactive for Aβ 4-42 something that has not been studied in these publications. Never the less, N-pyro-E-Aβ42 species have mechanistically been implicated in AD pathogenesis by accelerating Aβ aggregation kinetics since N-pyro-E-Aβ are more hydrophobic than the full-length species are more potent for self- and co- aggregation of less hydrophobic Aβ species including Aβ1-40 (51-54). Therefore, higher levels of AβpE3-42 and AβpE11-42 in cored and diffuse plaques in AD but not in diffuse plaques in CU-AP, likely reflect an important role of N-pyro-E-Aβ42 in seeding Aβ aggregation and early stages of plaque formation. This process likely involves hydrophobic priming that eventually leads to deposition of less hydrophobic species including Aβ1-40 that remain otherwise in solution.

Overall, these data indicate that Aβ1-42 and N-pyro-E-Aβ42 are relevant species in seeding pathology and that diffuse plaques represent an early stage of Aβ deposits that mature into cored plaques, and that this process involves the recruitment of more hydrophilic Aβ1-40 species over time. Here aggregation and functionalization of Aβ1-42 via N-terminal pyroglutamation are critical for seeding Aβ pathology in AD, while Aβ1-40 was shown to be associated with mature amyloid fibril formation (55). Further, Aβ1-40 was demonstrated to be significantly less potent for seeding amyloid fibril formation as compared to Aβ1-42 (45,56).

This notion is further supported by our observations for cerebrovascular amyloid pathology. Here, a strong localization of Aβ-40 peptide along with dominating q-FTAA binding was demonstrated for CAA in s-AD as well as in $tgAPP_{SWE}$. Further, in mice, similar to plaques, predominant Aβ1-40 deposition in CAA was found to increase with age. This suggests that CAA maturation is characterized by increased Aβ1-40 deposition.

This is in line with previous data, where development of CAA pathology has been shown to be associated with increased AD associated mutations that results in increased secretion of total Aβ, such as due to Swedish mutation in $tgAPP_{SWE}$ mice (32,57).

Further, Aβ1-42 as well as N-terminal Aβ truncations that are both prone to aggregation, have previously been shown to readily deposit as fibrillary diffuse plaques, while having no relevance in already seeded CAA or plaque nucleation (38,58). Similar to our findings, these previous studies suggest that with progressing pathology, Aβ species less prone to aggregation, dominated by Aβ1-40, do deposit on the pre-seeded aggregation sites, both in amyloid plaques - leading to core formation, as well as in the vasculature resulting in aggravated CAA pathology.

Importantly, the age-associated blue shift observed in CAA, caused by q-FTAA binding, along with increased Aβ1-40 deposition, indicates higher order aggregation represented by denser fibrillary structures, such as bundled multi-filamentous fibrils (12). These, denser, fibril structures might be associated with other physiological consequences, including stroke and hemorrhages. Indeed, CAA is associated with vascular Aβ clearance (59) and severe CAA pathology with frequent and spontaneous cerebral and lobar hemorrhages was described for both humans and transgenic AD mice (60-64). Given that hemorrhages occur due to decreasing flexibility in the endothelium of blood vessels (65), this suggests that differences in CAA associated hemorrhage between different AD mutations and are a consequence of higher rigidity of Aβ1-40 containing, mature fibrils. Indeed, Aβ1-40 fibrils were shown to be over 50 times less elastic than the Aβ1-42 fibrils (66) and this has been attributed to different β-sheet organization within each fibrillary layer of mature Aβ fibrils (66).

In summary, we identified that Aβ plaque polymorphism is associated with distinct Aβ peptide patterns. Specifically, we found that Aβ1-40 and not Aβ1-42 is the dominating species in mature senile plaques with cored morphology that

have been implicated in AD pathogenesis. Further, this plaque maturation was found to be associated with increased levels of Aβ3pE-42, which could indicate a hydrophobic priming of diffuse plaque morphotypes in AD through pyroglutamate modification of N-terminally truncated Aβ42.
A limitation of our study is the relatively small number of patients analyzed. These cross-sectional data provide initial, molecular insight in heterogenous plaque pathology on a chemical scale, not previously possible and are largely, verified by the longitudinal mouse data. Though, there is a strong motivation in using the here described technologies for expanded follow-up studies both for longitudinal human studies and mechanistical studies in mice.

Taken together our data suggest that diffuse deposits are immature precursors of cored plaques and that pyroglutamation of N-terminal Aβx-42, and Aβ1-40 deposition, are potentially critical events in priming and maturation of pathogenic Aβ from diffuse into cored plaques. These processes could underlie development of neurotoxic plaque pathology in AD and could hence provide a mechanistic target for potential intervention.

Experimental Procedures

Patient Samples

Fresh brain tissue samples were obtained from temporal cortex of 8 clinically and pathologically diagnosed sporadic AD cases (s-AD, AD1-AD8), and 4 non-demented CU-AP cases (CU-AP1 - CU-AP4) (Table S1). All cases were obtained through the brain donation program of the Queen Square Brain Bank for Neurological Disorders (QSBB), Department of Movement Disorders, UCL Institute of Neurology. The standard diagnostic criteria were used for the neuropathological diagnosis of AD (67-69). The demographic data for all cases are shown in Table S1. Ethical approval for the study was obtained from the Local Research Ethics Committee of the National Hospital for Neurology and Neurosurgery as well as the Institutional Review Board at the University of Gothenburg (Gothenburg, 04/16/2015; DNr 012-15). All studies abide by the Declaration of Helsinki principles.

AD Mouse Model.

Fresh brain tissue samples were obtained from 12-month-old (n=3) and 18-month-old (n=5) male transgenic AD mice ($tgAPP_{Swe}$). Animals were reared *ad libitum* at an animal facility at Uppsala University under a 12/12 light cycle (70). The animals were anesthetized with isoflurane and sacrificed by decapitation. The brains were dissected quickly with less than 3 min post mortem delay and frozen on dry ice. All animal procedures were approved by the ethical committee at Uppsala University, Uppsala, Sweden (DNr #C17/14) and performed in compliance with national and local animal care as well as in accordance with the principles of the Declaration of Helsinki.

LCO Staining.

Two previously validated LCO fluorophores, q-FTAA and h-FTAA, were used for the staining of the fresh-frozen tissue (10,13). Fresh-frozen human and mouse brain tissue was cut into 12µm thick sections on a cryostat microtome (Leica CM 1520, Leica Biosystems, Nussloch, Germany) at -18°C, consecutive sections were collected on 0.17 PEN membrane slides (Zeiss/P.A.L.M., Microlaser Technologies, Bernsried, Germany) and stored at -80°C. Prior to staining the sections were thawed in a desiccator and fixed at -20°C for 10 min using 95% ethanol, and double-stained with q-FTAA and h-FTAA (2.4µM q-FTAA and 0.77µM h-FTAA in PBS) similar to a previously described protocol (10,13). Sections were incubated for 30 min at RT in the dark, rinsed with milliQ water, and finally dried through desiccation.

Congo red and LCO Co-Staining

Congo red staining was performed on fresh frozen tissue sections (12 um) that were fixed in 99% ethanol and rehydrated through 10 minute dips in 70% ethanol, dH2O and PBS pH 7.3. Congo red staining of amyloid was performed as described, with few modifications (71). In short, tissue sections were first stained with Mayers Hematoxylin for 1 min, destained in tapwater and deionized water. Tissues were equilibrated in alkaline 80% EtOH for 20 min followed by Congo red staining solution for 20 min for mouse tissue and 2 h for human tissue. The Congo red staining solution was prepared by a freshly filtered 0.2 %

(w/v) Congo red in alkaline 80% ethanol with 1% NaCl. Destaining was performed in deionized water and PBS pH 7.3. Sections were mounted using transparent Dako fluorescence mounting medium.

Hyperspectral imaging of LCO stained tissue sections was performed using a Leica DM6000 B fluorescence microscope (Leica, Wetzlar, Germany) equipped with a SpectraCube module (Applied Spectral Imaging, Migdal Ha-Emek, Israel). Imaging of Congo red stained tissue sections was performed using a Nikon Eclipse 50i microscope with open, semi crossed and crossed polarizers respectively (Figure S2A-C).

Transmission Electron Microscopy

For EM, tissue samples were prepared by fixation, embedding and ultra-microtome sectioning. PFA fixed tissue was incubated at 4°C overnight with Karnovsky fixative, containing 2% formaldehyde (Sigma-Aldrich, Sweden), and 2% glutaraldehyde (Agar Scientific Ltd., UK) in 0.1M sodium cacodylate buffer (Agar Scientific Ltd., UK). Tissue was washed with 0.1M sodium cacodylate buffer and postfixed with 2% osmium tetroxide (Agar Scientific Ltd., UK) in 0.1M sodium cacodylate buffer at rum at room temperature in dark for 2h. Dehydration was done with rising concentrations of ethanol (50%, 70%, 95% and 99.5%) and later with 100% acetone and embedded in Agar 100 resin (Agar Scientific Ltd., UK). Semi-thin tissue sections were obtained with an ultra-microtome (Leica EM UC6), placed onto copper grids (PELCO GRIDS 200, Ted Pella, INC., USA), and post stained with uranyl acetate and Reynolds lead citrate.

Electron microscopy observations were carried out on a GAIA3 FIB-SEM work station using a STEM detector (GAIA3; Tescan, Brno-Kohoutovice, Czech Republic) at 30.0 kV (Chalmers Materials Analysis Laboratory (CMAL), Chalmers University of Technology, Gothenburg, Sweden). (Figure S2D)

Spectral Analysis and Laser Microdissection.

Spectral imaging was performed using LSM 710 NLO laser-scanning microscope equipped with a 34-channel QUASAR detector (Zeiss). A Plan-Apochromat 20x/0.8 (WD= 0.55 mm), ∞/0.17 objective was used for spectral imaging of amyloid deposits prior to their isolation. Continuous emission was acquired in the range of 405 to 750nm (10,13). Linear unmixing, a function within the Zen 2011 (Zeiss) software, was used to differentiate between the true q-FTAA and h-FTAA fluorescent signals in the double stained samples, and distinguish between true LCO fluorescence spectrum and unwanted autofluorescence, from for instance lipofuscin (13). For hyperspectral differentiation based on the hyperspectral line-scan, an in-house developed macro for ImageJ (http://rsb.info.nih.gov/ij/) was used. The macro allows the detection of the wavelength showing the normalized intensity for each position (pixel) in the region of interest. Amyloid plaques and cerebral amyloid angiopathies were chosen randomly, and were subcategorized into cored and diffuse deposits, based on their line-scan profiles. Plaques were annotated based on their LCO profile by three independent investigators. In s-AD tissue, a total of 200-250 cored plaques and 200-250 diffuse plaques, and ~50 CAA deposits, were collected for from 5 consecutive, temporal cortical sections. In CU-AP tissue, a total of 200-250 diffuse plaques were collected for from 5 consecutive, temporal cortical sections. This was sufficient for extraction and provided the necessary MS signal. For transgenic mice a number of 15-20 cored plaques and 15-20 diffuse plaques were each collected for cortex and hippocampus from 5 consecutive, sagittal sections. Here, the number of plaques was smaller as the amyloid content in transgenics is significantly higher due to over expression. In addition, a number 15-25 CAA deposits were collected per animal from 5 consecutive, sagittal sections per animal.

By investigating plaques at different sections for each patient- or animal brain sample, we ensured that only truly diffuse or truly cored plaques were excised. This to prevent classification of a diffuse corona of a cored plaque as a diffuse plaque, as truly diffuse plaques span over several sections. At the same time, this also provided a representative coverage of biological variation within each brain sample, by including plaques from different sections.

Annotated plaques were then excised by laser microdissection pressure catapulting.

Microdissection was done using a PALM Microbeam LMPC microscope (Zeiss) equipped with a 355 nm pulsed UV-laser. The spectrally differentiated Aβ plaque subpopulations, and CAA were collected in Adhesive Cap 500 opaque tubes (Zeiss) and stored at -20°C prior to extraction.

Aβ Immunoprecipitation, Aβ Quantification, Mass Spectrometry.

To the isolated amyloid aggregates 50µL of 70% formic acid, with 5mM EDTA was added, samples were sonicated for 5 minutes, incubated for 1 h at 24°C. The samples were then neutralized to pH 7 using 0.5M Tris. Aβ peptides were than purified through immunoprecipitation using Aβ-specific antibodies (antibodies 6E10 and 4G8, Signet Laboratories), coupled to magnetic Dynabeads M-280 Sheep Anti-Mouse (Invitrogen) as described previously (13,72). The supernatant was collected and dried through lyophilization. Mass spectrometric comparison of the samples was performed using a MALDI TOF/TOF UltrafleXtreme instrument (Bruker Daltonics, Bremen, Germany) as described previously (13,72). Further, to verify the identity of the observed peptides, an LC-MS/MS analysis, using alkaline mobile phase, of brain was carried out using a Q Exactive quadrupole-orbitrap hybrid mass spectrometer equipped with a heated electrospray ionization source (HESI-II) (Thermo Scientific) and UltiMate 3000 binary pump, column oven, and autosampler (Thermo Scientific), as previously described (73), but with the Q Exactive operated in data dependent mode. Briefly, the resolution settings were 70,000 and target values were 1×10^6 both for MS and MS/MS acquisitions. Acquisitions were performed with 1 microscan/acquisition. Precursor isolation width was 3 m/z units and ions were fragmented by so-called higher energy collision induced dissociation (HCD) at a normalized collision energy (NCE) of 25.

Data Processing and Statistical Analysis.

For statistical analysis, individual spectra were exported as csv files from FlexAnalysis (v.3.0, Bruker Daltonics) and imported into Origin (v. 8.1 OriginLab, Northampton, MA, USA). Bin borders were used for area under curve (AUC) peak integration within each bin using an in-house developed R script, as described before (74). Individual peptide signal was normalized to all detected and verified peptides. Analysis of individual peptide signals and comparisons between the groups were performed with paired (s-AD, same animal) and unpaired (s-AD/CU-AP, and between ages), two tailed t-test, correlation between the variables was accessed using Pearson regression analysis. A p-value threshold of 0.05 was used for assessment of the statistical significance. Statistical analysis was performed using GraphPad Prism (v.7). Spectra were deconvoluted using Mascot Distiller before submission to database search using the Mascot search engine (both Matrix Science) as described previously (75). The MS/MS spectra were searched toward the SwissProt database containing the mutant human APP sequence using the following search parameters: taxonomy; Homo sapiens, precursor mass ± 15 ppm; fragment mass ± 0.05 Da; no enzyme; no fixed modifications; variable modifications including deamidated (NQ), Glu->pyro-Glu (N-term E), oxidation (M); instrument default. For illustration, spectra were processed and searched using PEAKS Studio 8.5 (Bio-informatics Solutions, Inc., Waterloo, ON, Canada) (Figure S3-S5).

Tissue Preparation and MALDI imaging MS of Aβ Peptides

For MALDI imaging, consecutive tissue sections to those collected for LMPC on PEN membrane slides, were thaw mounted on conductive indium tin oxide (ITO) glass slides (Bruker Daltonics). A series of sequential washes of 100% EtOH (60 s), 70% EtOH (30 s), Carnoy's fluid (6:3:1 EtOH/chloroform/acetic acid) (110 s), 100% EtOH (15 s), H_2O with 0.2% TFA (60 s), and 100% EtOH (15 s) was carried out. Tissue was subjected to formic acid vapor for 20 minutes. 2,5-Dihydroxyacetophenone (2,5-DHAP) was used as matrix compound and applied using a TM Sprayer. A matrix solution of 15 mg/mL 2,5-DHAP in 70% ACN/2%CH_3COOH/2%TFA was sprayed onto the tissue sections using the following instrumental parameters: nitrogen flow (10 psi), spray temperature (75°C), nozzle height (40 mm), eight passes with offsets and rotations, and spray velocity (1000 mm/min), and isocratic flow of 100µL/min using 70% ACN as pushing solvent. Following the matrix deposition, the preparations

were recrystallized with 5% methanol at 85°C, for 3min as described previously (76,77).
MALDI-imaging MS (IMS) was performed on a UltrafleXtreme instrument equipped with SmartBeam II Nd:YAG/355 nm laser as described previously (77). For verification of Aβ peptide distribution in tissue, image data were reconstructed; total ion current (TIC) normalized and visualized using the Flex Imaging v3.0 software (Bruker Daltonics).

Acknowledgements: We thank the staff at Centre for Cellular Imaging (CCI), Core Facilities, The Sahlgrenska Academy at the University of Gothenburg for help with development of hyperspectral imaging paradigm and microscopy expertise. The Swedish Research Council VR (#2014-6447, #2018-02181 JH; #2012-1593, SS; #2013-2546, HZ; #2016-00748, KPRN), the European Research Council (#681712, HZ), Alzheimerfonden (JH, SS, KB, SN, DS, PH), Demensfonden (JH, WM), Hjärnfonden (SS, KB, PH), Jeanssons Stiftelsen (JH), Ahlén Stiftelsen (JH, SS, DS), Stiftelsen Gamla Tjänarinnor (JH, KB, WM, DS, GB), Stohnes Stiftelse (JH, GB, SS, DS), Torsten Söderberg Foundation (KB, SS), the Swedish Foundation for Strategic Research SSF (KPRN) and the Göran Gustafsson Foundation (PH) are acknowledged for financial support. TL holds an Alzheimer's Research UK (ARUK) Senior Fellowship.

Conflict of Interest: The authors declare that they have no conflicts of interest with the contents of this article.

Author Contribution: J.H., W.M conceived and designed the study. S.S., D.S provided the mouse brain samples. T.L. selected and provided the human brain samples. W.M., S.N., P.H. and G.B. performed experiments. W.M., P.W., T.L. L.G., G.B., J.H. analyzed and interpreted the data. W.M., S.N., P.W., T.L., G.B., S.S., D.S., I.K., D.B., L.G., K.P.R.N., P.H., K.B., H.Z. and J.H. discussed the data. W.M., K.B., H.Z. and J.H. wrote the manuscript. All authors approved the final version of the manuscript.

References

1. Huang, T. H., Yang, D. S., Fraser, P. E., and Chakrabartty, A. (2000) Alternate aggregation pathways of the Alzheimer beta-amyloid peptide. An in vitro model of preamyloid. *J Biol Chem* **275**, 36436-36440

2. Jiang, D., Rauda, I., Han, S., Chen, S., and Zhou, F. (2012) Aggregation pathways of the amyloid beta(1-42) peptide depend on its colloidal stability and ordered beta-sheet stacking. *Langmuir* **28**, 12711-12721

3. Karran, E., and De Strooper, B. (2016) The amyloid cascade hypothesis: are we poised for success or failure? *J Neurochem* **139 Suppl 2**, 237-252

4. Dickson, T. C., and Vickers, J. C. (2001) The morphological phenotype of beta-amyloid plaques and associated neuritic changes in Alzheimer's disease. *Neuroscience* **105**, 99-107

5. Ikeda, S., Allsop, D., and Glenner, G. G. (1989) Morphology and distribution of plaque and related deposits in the brains of Alzheimer's disease and control cases. An immunohistochemical study using amyloid beta-protein antibody. *Laboratory investigation; a journal of technical methods and pathology* **60**, 113-122

6. Thal, D. R., Capetillo-Zarate, E., Del Tredici, K., and Braak, H. (2006) The development of amyloid beta protein deposits in the aged brain. *Science of aging knowledge environment : SAGE KE* **2006**, re1

7. Yamaguchi, H., Hirai, S., Morimatsu, M., Shoji, M., and Ihara, Y. (1988) A variety of cerebral amyloid deposits in the brains of the Alzheimer-type dementia demonstrated by beta protein immunostaining. *Acta neuropathologica* **76**, 541-549

8. Tagliavini, F., Giaccone, G., Frangione, B., and Bugiani, O. (1988) Preamyloid deposits in the cerebral cortex of patients with Alzheimer's disease and nondemented individuals. *Neuroscience letters* **93**, 191-196

9. Portelius, E., Bogdanovic, N., Gustavsson, M. K., Volkmann, I., Brinkmalm, G., Zetterberg, H., Winblad, B., and Blennow, K. (2010) Mass spectrometric characterization of brain amyloid beta isoform signatures in familial and sporadic Alzheimer's disease. *Acta neuropathologica* **120**, 185-193

10. Nystrom, S., Psonka-Antonczyk, K. M., Ellingsen, P. G., Johansson, L. B., Reitan, N., Handrick, S., Prokop, S., Heppner, F. L., Wegenast-Braun, B. M., Jucker, M., Lindgren, M., Stokke, B. T., Hammarstrom, P., and Nilsson, K. P. (2013) Evidence for age-dependent in vivo conformational rearrangement within Abeta amyloid deposits. *ACS Chem Biol* **8**, 1128-1133

11. Klingstedt, T., Blechschmidt, C., Nogalska, A., Prokop, S., Haggqvist, B., Danielsson, O., Engel, W. K., Askanas, V., Heppner, F. L., and Nilsson, K. P. (2013) Luminescent conjugated oligothiophenes for sensitive fluorescent assignment of protein inclusion bodies. *Chembiochem* **14**, 607-616

12. Psonka-Antonczyk, K. M., Hammarstrom, P., Johansson, L. B., Lindgren, M., Stokke, B. T., Nilsson, K. P., and Nystrom, S. (2016) Nanoscale Structure and Spectroscopic Probing of Abeta1-40 Fibril Bundle Formation. *Frontiers in chemistry* **4**, 44

13. Rasmussen, J., Mahler, J., Beschorner, N., Kaeser, S. A., Hasler, L. M., Baumann, F., Nystrom, S., Portelius, E., Blennow, K., Lashley, T., Fox, N. C., Sepulveda-Falla, D., Glatzel, M., Oblak, A. L., Ghetti, B., Nilsson, K. P. R., Hammarstrom, P., Staufenbiel, M., Walker, L. C., and Jucker, M. (2017) Amyloid polymorphisms constitute distinct clouds of conformational variants in different etiological subtypes of Alzheimer's disease. *Proceedings of the National Academy of Sciences of the United States of America* **114**, 13018-13023

14. Watts, J. C., Condello, C., Stöhr, J., Oehler, A., Lee, J., DeArmond, S. J., Lannfelt, L., Ingelsson, M., Giles, K., and Prusiner, S. B. (2014) Serial propagation of distinct strains of Aβ prions from Alzheimer's disease patients. *Proceedings of the National Academy of Sciences of the United States of America* **111**, 10323-10328

15. Condello, C., Lemmin, T., Stohr, J., Nick, M., Wu, Y., Maxwell, A. M., Watts, J. C., Caro, C. D., Oehler, A., Keene, C. D., Bird, T. D., van Duinen, S. G., Lannfelt, L., Ingelsson, M., Graff, C., Giles, K., DeGrado, W. F., and Prusiner, S. B. (2018) Structural heterogeneity and intersubject variability of Abeta in familial and sporadic Alzheimer's disease. *Proceedings of the National Academy of Sciences of the United States of America* **115**, E782-e791

16. McGowan, E., Pickford, F., Kim, J., Onstead, L., Eriksen, J., Yu, C., Skipper, L., Murphy, M. P., Beard, J., Das, P., Jansen, K., Delucia, M., Lin, W. L., Dolios, G., Wang, R., Eckman, C. B., Dickson, D. W., Hutton, M., Hardy, J., and Golde, T. (2005) Abeta42 is essential for parenchymal and vascular amyloid deposition in mice. *Neuron* **47**, 191-199

17. Lendel, C., Bjerring, M., Dubnovitsky, A., Kelly, R. T., Filippov, A., Antzutkin, O. N., Nielsen, N. C., and Hard, T. (2014) A hexameric peptide barrel as building block of amyloid-beta protofibrils. *Angew Chem Int Ed Engl* **53**, 12756-12760

18. Bitan, G., Kirkitadze, M. D., Lomakin, A., Vollers, S. S., Benedek, G. B., and Teplow, D. B. (2003) Amyloid beta -protein (Abeta) assembly: Abeta 40 and Abeta 42 oligomerize through distinct pathways. *Proceedings of the National Academy of Sciences of the United States of America* **100**, 330-335

19. Esbjorner, E. K., Chan, F., Rees, E., Erdelyi, M., Luheshi, L. M., Bertoncini, C. W., Kaminski, C. F., Dobson, C. M., and Kaminski Schierle, G. S. (2014) Direct observations of amyloid beta self-assembly in live cells provide insights into differences in the kinetics of Abeta(1-40) and Abeta(1-42) aggregation. *Chemistry & biology* **21**, 732-742

20. Dickson, D. W., Crystal, H. A., Mattiace, L. A., Masur, D. M., Blau, A. D., Davies, P., Yen, S. H., and Aronson, M. K. (1992) Identification of normal and pathological aging in prospectively studied nondemented elderly humans. *Neurobiol Aging* **13**, 179-189

21. Jack, C. R., Jr., Bennett, D. A., Blennow, K., Carrillo, M. C., Dunn, B., Haeberlein, S. B., Holtzman, D. M., Jagust, W., Jessen, F., Karlawish, J., Liu, E., Molinuevo, J. L., Montine, T., Phelps, C., Rankin, K. P., Rowe, C. C., Scheltens, P., Siemers, E., Snyder, H. M., and Sperling, R. (2018) NIA-AA Research Framework: Toward a biological definition of Alzheimer's disease. *Alzheimer's & dementia : the journal of the Alzheimer's Association* **14**, 535-562

22. Lord, A., Kalimo, H., Eckman, C., Zhang, X.-Q., Lannfelt, L., and Nilsson, L. N. G. (2006) The Arctic Alzheimer mutation facilitates early intraneuronal Aβ aggregation and senile plaque formation in transgenic mice. *Neurobiology of Aging* **27**, 67-77

23. Nilsson, K. P., Aslund, A., Berg, I., Nystrom, S., Konradsson, P., Herland, A., Inganas, O., Stabo-Eeg, F., Lindgren, M., Westermark, G. T., Lannfelt, L., Nilsson, L. N., and Hammarstrom, P. (2007) Imaging distinct conformational states of amyloid-beta fibrils in Alzheimer's disease using novel luminescent probes. *ACS Chem Biol* **2**, 553-560

24. Ellingsen, P. G., Nystrom, S., Reitan, N. K., and Lindgren, M. (2013) Spectral correlation analysis of amyloid beta plaque inhomogeneity from double staining experiments. *J Biomed Opt* **18**, 101313

25. Philipson, O., Hammarstrom, P., Nilsson, K. P., Portelius, E., Olofsson, T., Ingelsson, M., Hyman, B. T., Blennow, K., Lannfelt, L., Kalimo, H., and Nilsson, L. N. (2009) A highly insoluble state of Abeta similar to that of Alzheimer's disease brain is found in Arctic APP transgenic mice. *Neurobiol Aging* **30**, 1393-1405

26. Iwatsubo, T., Odaka, A., Suzuki, N., Mizusawa, H., Nukina, N., and Ihara, Y. (1994) Visualization of A beta 42(43) and A beta 40 in senile plaques with end-specific A beta monoclonals: evidence that an initially deposited species is A beta 42(43). *Neuron* **13**, 45-53

27. Kuo, Y. M., Beach, T. G., Sue, L. I., Scott, S., Layne, K. J., Kokjohn, T. A., Kalback, W. M., Luehrs, D. C., Vishnivetskaya, T. A., Abramowski, D., Sturchler-Pierrat, C., Staufenbiel, M., Weller, R. O., and Roher, A. E. (2001) The evolution of A beta peptide burden in the APP23 transgenic mice: implications for A beta deposition in Alzheimer disease. *Mol Med* **7**, 609-618

28. Gu, L., and Guo, Z. (2013) Alzheimer's Abeta42 and Abeta40 peptides form interlaced amyloid fibrils. *J Neurochem* **126**, 305-311

29. Kumar-Singh, S. (2008) Cerebral amyloid angiopathy: pathogenetic mechanisms and link to dense amyloid plaques. *Genes, brain, and behavior* **7 Suppl 1**, 67-82

30. Hsiao, K., Chapman, P., Nilsen, S., Eckman, C., Harigaya, Y., Younkin, S., Yang, F., and Cole, G. (1996) Correlative memory deficits, Abeta elevation, and amyloid plaques in transgenic mice. *Science (New York, N.Y.)* **274**, 99-102

31. Sturchler-Pierrat, C., Abramowski, D., Duke, M., Wiederhold, K. H., Mistl, C., Rothacher, S., Ledermann, B., Burki, K., Frey, P., Paganetti, P. A., Waridel, C., Calhoun, M. E., Jucker, M., Probst, A., Staufenbiel, M., and Sommer, B. (1997) Two amyloid precursor protein transgenic mouse models with Alzheimer disease-like pathology. *Proceedings of the National Academy of Sciences of the United States of America* **94**, 13287-13292

32. Kumar-Singh, S., Pirici, D., McGowan, E., Serneels, S., Ceuterick, C., Hardy, J., Duff, K., Dickson, D., and Van Broeckhoven, C. (2005) Dense-core plaques in Tg2576 and PSAPP mouse models of Alzheimer's disease are centered on vessel walls. *The American journal of pathology* **167**, 527-543

33. Blennow, K., Hampel, H., Weiner, M., and Zetterberg, H. (2010) Cerebrospinal fluid and plasma biomarkers in Alzheimer disease. *Nature reviews. Neurology* **6**, 131-144

34. Fagan, A. M., Mintun, M. A., Mach, R. H., Lee, S. Y., Dence, C. S., Shah, A. R., LaRossa, G. N., Spinner, M. L., Klunk, W. E., Mathis, C. A., DeKosky, S. T., Morris, J. C., and Holtzman, D. M. (2006) Inverse relation between in vivo amyloid imaging load and cerebrospinal fluid Abeta42 in humans. *Annals of neurology* **59**, 512-519

35. Strozyk, D., Blennow, K., White, L. R., and Launer, L. J. (2003) CSF Abeta 42 levels correlate with amyloid-neuropathology in a population-based autopsy study. *Neurology* **60**, 652-656

36. Wang, J., Dickson, D. W., Trojanowski, J. Q., and Lee, V. M. (1999) The levels of soluble versus insoluble brain Abeta distinguish Alzheimer's disease from normal and pathologic aging. *Experimental neurology* **158**, 328-337

37. Mori, H., Takio, K., Ogawara, M., and Selkoe, D. J. (1992) Mass spectrometry of purified amyloid beta protein in Alzheimer's disease. *J Biol Chem* **267**, 17082-17086

38. Fukumoto, H., Asami-Odaka, A., Suzuki, N., and Iwatsubo, T. (1996) Association of A beta 40-positive senile plaques with microglial cells in the brains of patients with Alzheimer's disease and in non-demented aged individuals. *Neurodegeneration : a journal for neurodegenerative disorders, neuroprotection, and neuroregeneration* **5**, 13-17

39. Verbeek, M. M., Kremer, B. P., Rikkert, M. O., Van Domburg, P. H., Skehan, M. E., and Greenberg, S. M. (2009) Cerebrospinal fluid amyloid beta(40) is decreased in cerebral amyloid angiopathy. *Annals of neurology* **66**, 245-249

40. Güntert, A., Döbeli, H., and Bohrmann, B. (2006) High sensitivity analysis of amyloid-beta peptide composition in amyloid deposits from human and PS2APP mouse brain. *Neuroscience* **143**, 461-475

41. Kawarabayashi, T., Younkin, L. H., Saido, T. C., Shoji, M., Ashe, K. H., and Younkin, S. G. (2001) Age-dependent changes in brain, CSF, and plasma amyloid (beta) protein in the Tg2576 transgenic mouse model of Alzheimer's disease. *J Neurosci* **21**, 372-381

42. Heilbronner, G., Eisele, Y. S., Langer, F., Kaeser, S. A., Novotny, R., Nagarathinam, A., Aslund, A., Hammarstrom, P., Nilsson, K. P., and Jucker, M. (2013) Seeded strain-like transmission of beta-amyloid morphotypes in APP transgenic mice. *EMBO reports* **14**, 1017-1022

43. Cummings, D. M., Liu, W., Portelius, E., Bayram, S., Yasvoina, M., Ho, S. H., Smits, H., Ali, S. S., Steinberg, R., Pegasiou, C. M., James, O. T., Matarin, M., Richardson, J. C., Zetterberg, H., Blennow, K., Hardy, J. A., Salih, D. A., and Edwards, F. A. (2015) First effects of rising amyloid-beta in transgenic mouse brain: synaptic transmission and gene expression. *Brain : a journal of neurology* **138**, 1992-2004

44. Terai, K., Iwai, A., Kawabata, S., Sasamata, M., Miyata, K., and Yamaguchi, T. (2001) Apolipoprotein E deposition and astrogliosis are associated with maturation of beta-amyloid plaques in betaAPPswe transgenic mouse: Implications for the pathogenesis of Alzheimer's disease. *Brain research* **900**, 48-56

45. Ahmed, M., Davis, J., Aucoin, D., Sato, T., Ahuja, S., Aimoto, S., Elliott, J. I., Van Nostrand, W. E., and Smith, S. O. (2010) Structural conversion of neurotoxic amyloid-beta(1-42) oligomers to fibrils. *Nature structural & molecular biology* **17**, 561-567

46. Lord, A., Philipson, O., Klingstedt, T., Westermark, G., Hammarstrom, P., Nilsson, K. P., and Nilsson, L. N. (2011) Observations in APP bitransgenic mice suggest that diffuse and compact plaques form via independent processes in Alzheimer's disease. *The American journal of pathology* **178**, 2286-2298

47. Meyer-Luehmann, M., Spires-Jones, T. L., Prada, C., Garcia-Alloza, M., de Calignon, A., Rozkalne, A., Koenigsknecht-Talboo, J., Holtzman, D. M., Bacskai, B. J., and Hyman, B. T. (2008) Rapid appearance and local toxicity of amyloid-beta plaques in a mouse model of Alzheimer's disease. *Nature* **451**, 720-724

48. Saido, T. C., Iwatsubo, T., Mann, D. M., Shimada, H., Ihara, Y., and Kawashima, S. (1995) Dominant and differential deposition of distinct beta-amyloid peptide species, A beta N3(pE), in senile plaques. *Neuron* **14**, 457-466

49. Kuo, Y. M., Emmerling, M. R., Woods, A. S., Cotter, R. J., and Roher, A. E. (1997) Isolation, chemical characterization, and quantitation of A beta 3-pyroglutamyl peptide from neuritic plaques and vascular amyloid deposits. *Biochemical and biophysical research communications* **237**, 188-191

50. Harigaya, Y., Saido, T. C., Eckman, C. B., Prada, C. M., Shoji, M., and Younkin, S. G. (2000) Amyloid beta protein starting pyroglutamate at position 3 is a major component of the amyloid deposits in the Alzheimer's disease brain. *Biochemical and biophysical research communications* **276**, 422-427

51. D'Arrigo, C., Tabaton, M., and Perico, A. (2009) N-terminal truncated pyroglutamyl beta amyloid peptide Abetapy3-42 shows a faster aggregation kinetics than the full-length Abeta1-42. *Biopolymers* **91**, 861-873

52. Wirths, O., Bethge, T., Marcello, A., Harmeier, A., Jawhar, S., Lucassen, P. J., Multhaup, G., Brody, D. L., Esparza, T., Ingelsson, M., Kalimo, H., Lannfelt, L., and Bayer, T. A. (2010) Pyroglutamate Abeta pathology in APP/PS1KI mice, sporadic and familial Alzheimer's disease cases. *Journal of neural transmission (Vienna, Austria : 1996)* **117**, 85-96

53. Schilling, S., Zeitschel, U., Hoffmann, T., Heiser, U., Francke, M., Kehlen, A., Holzer, M., Hutter-Paier, B., Prokesch, M., Windisch, M., Jagla, W., Schlenzig, D., Lindner, C., Rudolph, T., Reuter, G., Cynis, H., Montag, D., Demuth, H. U., and Rossner, S. (2008) Glutaminyl cyclase inhibition attenuates pyroglutamate Abeta and Alzheimer's disease-like pathology. *Nature medicine* **14**, 1106-1111

54. He, W., and Barrow, C. J. (1999) The A beta 3-pyroglutamyl and 11-pyroglutamyl peptides found in senile plaque have greater beta-sheet forming and aggregation propensities in vitro than full-length A beta. *Biochemistry* **38**, 10871-10877

55. Shin, R.-W., Ogino, K., Kondo, A., Saido, T. C., Trojanowski, J. Q., Kitamoto, T., and Tateishi, J. (1997) Amyloid β-Protein (Aβ) 1–40 But Not Aβ1–42 Contributes to the Experimental Formation of Alzheimer Disease Amyloid Fibrils in Rat Brain. *The Journal of Neuroscience* **17**, 8187-8193

56. Schmidt, M., Sachse, C., Richter, W., Xu, C., Fandrich, M., and Grigorieff, N. (2009) Comparison of Alzheimer Abeta(1-40) and Abeta(1-42) amyloid fibrils reveals similar protofilament structures. *Proceedings of the National Academy of Sciences of the United States of America* **106**, 19813-19818

57. Mann, D. M., Iwatsubo, T., Ihara, Y., Cairns, N. J., Lantos, P. L., Bogdanovic, N., Lannfelt, L., Winblad, B., Maat-Schieman, M. L., and Rossor, M. N. (1996) Predominant deposition of amyloid-beta 42(43) in plaques in cases of Alzheimer's disease and hereditary cerebral hemorrhage associated with mutations in the amyloid precursor protein gene. *The American journal of pathology* **148**, 1257-1266

58. Pike, C. J., Overman, M. J., and Cotman, C. W. (1995) Amino-terminal deletions enhance aggregation of beta-amyloid peptides in vitro. *J Biol Chem* **270**, 23895-23898

59. Weller, R. O., Massey, A., Newman, T. A., Hutchings, M., Kuo, Y. M., and Roher, A. E. (1998) Cerebral amyloid angiopathy: amyloid beta accumulates in putative interstitial fluid drainage pathways in Alzheimer's disease. *The American journal of pathology* **153**, 725-733

60. Levy, E., Carman, M. D., Fernandez-Madrid, I. J., Power, M. D., Lieberburg, I., van Duinen, S. G., Bots, G. T., Luyendijk, W., and Frangione, B. (1990) Mutation of the Alzheimer's disease amyloid gene in hereditary cerebral hemorrhage, Dutch type. *Science (New York, N.Y.)* **248**, 1124-1126

61. Nilsberth, C., Westlind-Danielsson, A., Eckman, C. B., Condron, M. M., Axelman, K., Forsell, C., Stenh, C., Luthman, J., Teplow, D. B., Younkin, S. G., Naslund, J., and Lannfelt, L. (2001) The 'Arctic' APP mutation (E693G) causes Alzheimer's disease by enhanced Abeta protofibril formation. *Nature neuroscience* **4**, 887-893

62. Grabowski, T. J., Cho, H. S., Vonsattel, J. P., Rebeck, G. W., and Greenberg, S. M. (2001) Novel amyloid precursor protein mutation in an Iowa family with dementia and severe cerebral amyloid angiopathy. *Annals of neurology* **49**, 697-705

63. Cai, X. D., Golde, T. E., and Younkin, S. G. (1993) Release of excess amyloid beta protein from a mutant amyloid beta protein precursor. *Science (New York, N.Y.)* **259**, 514-516

64. Citron, M., Oltersdorf, T., Haass, C., McConlogue, L., Hung, A. Y., Seubert, P., Vigo-Pelfrey, C., Lieberburg, I., and Selkoe, D. J. (1992) Mutation of the beta-amyloid precursor protein in familial Alzheimer's disease increases beta-protein production. *Nature* **360**, 672-674

65. Gibbons, G. H., and Dzau, V. J. (1994) The emerging concept of vascular remodeling. *The New England journal of medicine* **330**, 1431-1438

66. Dong, M., Paul, T. J., Hoffmann, Z., Chan, K., Hu, D., Ai, H., and Prabhakar, R. (2016) Structural and Material Properties of Amyloid Abeta40/42 Fibrils. *Chemphyschem : a European journal of chemical physics and physical chemistry* **17**, 2558-2566

67. Thal, D. R., Rub, U., Orantes, M., and Braak, H. (2002) Phases of A beta-deposition in the human brain and its relevance for the development of AD. *Neurology* **58**, 1791-1800

68. Braak, H., and Braak, E. (1991) Neuropathological stageing of Alzheimer-related changes. *Acta neuropathologica* **82**, 239-259

69. Montine, T. J., Phelps, C. H., Beach, T. G., Bigio, E. H., Cairns, N. J., Dickson, D. W., Duyckaerts, C., Frosch, M. P., Masliah, E., Mirra, S. S., Nelson, P. T., Schneider, J. A., Thal, D. R., Trojanowski, J. Q., Vinters, H. V., and Hyman, B. T. (2012) National Institute on Aging-Alzheimer's Association guidelines for the neuropathologic assessment of Alzheimer's disease: a practical approach. *Acta neuropathologica* **123**, 1-11

70. Lord, A., Kalimo, H., Eckman, C., Zhang, X. Q., Lannfelt, L., and Nilsson, L. N. (2006) The Arctic Alzheimer mutation facilitates early intraneuronal Abeta aggregation and senile plaque formation in transgenic mice. *Neurobiol Aging* **27**, 67-77

71. Westermark, G. T., Johnson, K. H., and Westermark, P. (1999) Staining methods for identification of amyloid in tissue. *Methods in enzymology* **309**, 3-25

72. Portelius, E., Tran, A. J., Andreasson, U., Persson, R., Brinkmalm, G., Zetterberg, H., Blennow, K., and Westman-Brinkmalm, A. (2007) Characterization of amyloid beta peptides in cerebrospinal fluid by an automated immunoprecipitation procedure followed by mass spectrometry. *Journal of proteome research* **6**, 4433-4439

73. Pannee, J., Portelius, E., Minthon, L., Gobom, J., Andreasson, U., Zetterberg, H., Hansson, O., and Blennow, K. (2016) Reference measurement procedure for CSF amyloid beta (Abeta)1-42 and the CSF Abeta1-42 /Abeta1-40 ratio - a cross-validation study against amyloid PET. *J Neurochem* **139**, 651-658

74. Hanrieder, J., Ljungdahl, A., Falth, M., Mammo, S. E., Bergquist, J., and Andersson, M. (2011) L-DOPA-induced dyskinesia is associated with regional increase of striatal dynorphin peptides as elucidated by imaging mass spectrometry. *Molecular & cellular proteomics : MCP* **10**, M111 009308

75. Brinkmalm, G., Portelius, E., Ohrfelt, A., Mattsson, N., Persson, R., Gustavsson, M. K., Vite, C. H., Gobom, J., Mansson, J. E., Nilsson, J., Halim, A., Larson, G., Ruetschi, U., Zetterberg, H., Blennow, K., and Brinkmalm, A. (2012) An online nano-LC-ESI-FTICR-MS method for comprehensive characterization of endogenous fragments from amyloid beta and amyloid precursor protein in human and cat cerebrospinal fluid. *Journal of mass spectrometry : JMS* **47**, 591-603

76. Yang, J., and Caprioli, R. M. (2011) Matrix Sublimation/Recrystallization for Imaging Proteins by Mass Spectrometry at High Spatial Resolution. *Analytical Chemistry* **83**, 5728-5734

77. Kaya, I., Brinet, D., Michno, W., Başkurt, M., Zetterberg, H., Blenow, K., and Hanrieder, J. (2017) Novel Trimodal MALDI Imaging Mass Spectrometry (IMS3) at 10 μm Reveals Spatial Lipid and Peptide Correlates Implicated in Aβ Plaque Pathology in Alzheimer's Disease. *ACS Chemical Neuroscience* **8**, 2778-2790

Figures

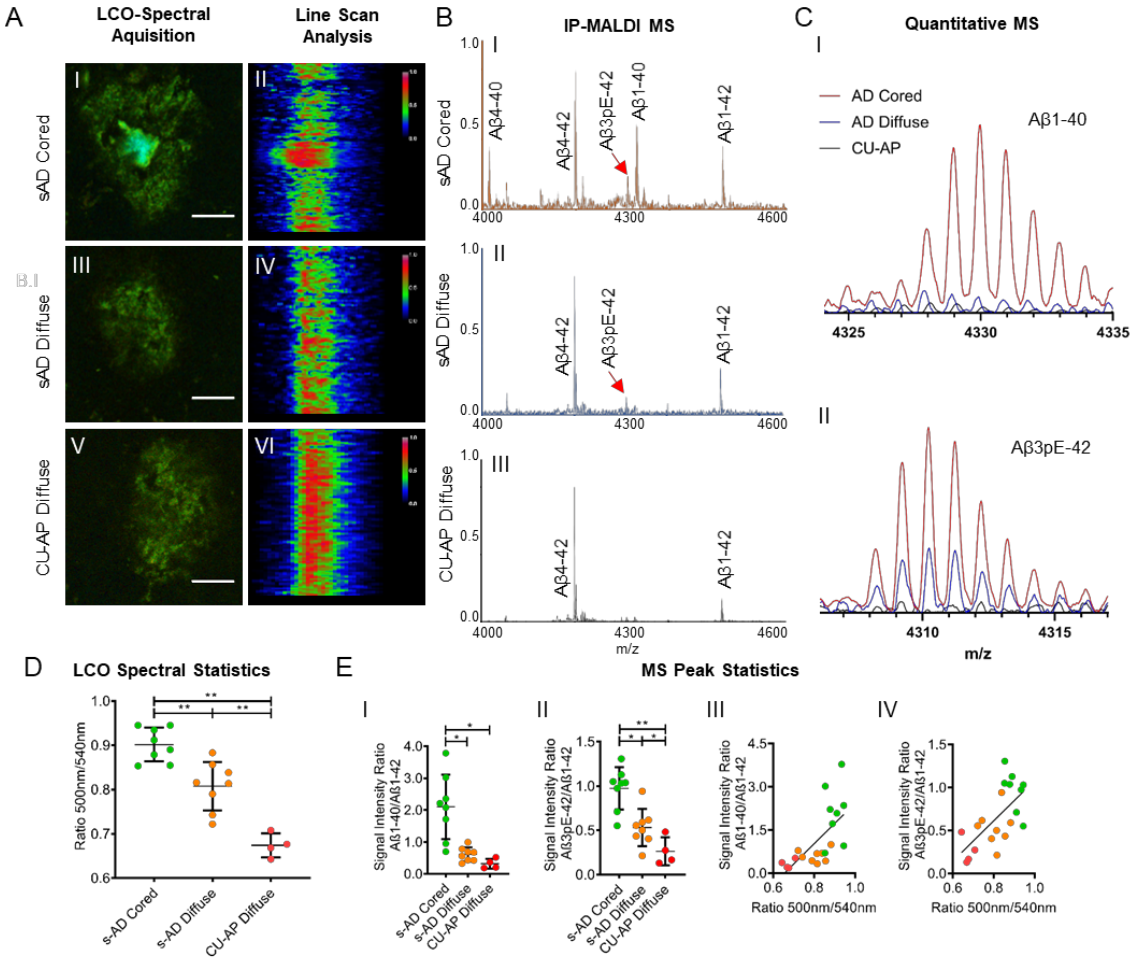

Figure 1. Spectral and mass spectrometric analysis of amyloid deposits in s-AD and CU-AP patients. (A) LCO Microscopy: Double staining was performed with q-FTAA and h-FTAA. Cross-sectional emission profile of cored- (A.I, A.II) and diffuse- plaques in s-AD (A.III, A.IV) in comparison to diffuse plaques in CU-AP patients (A.V, A.VI). Hyperspectrally classified plaques were then excised with laser microdissection and extracted with formic acid followed by immunoprecipitation and MALDI mass spectrometry (IP-MALDI MS). (B) MALDI MS: MALDI mass spectra for immunoprecipitated (IP) plaque extracts from laser micro-dissected cored plaques (B.I) and diffuse plaques (B.II) in a s-AD, and diffuse plaques in CU-AP patients (B.III). (C) Zoomed MALDI MS traces: Overlay of average mass spectra for Aβ1-40 (C.I) and AβpE3-42 (C.II), indicating higher levels of Aβ1-40 in cored plaques (red) compared to diffuse plaques and increased levels of AβpE3-42 in s-AD (red and blue) as compared to CU-AP (black). (D) Statistics on hyperspectral emission ratio values (500nm/540nm) corresponding to the degree of q- and h-FTAA content. (E) Statistics on Aβ1-40 and AβpE3-42 MS signal in between plaque groups (E.I, E.II) and correlation with 500nm/540nm emission ratio for Aβ1-40/Aβ1-42 (R^2=0.43, p<0.005) (E.III); AβpE3-42/Aβ1-42 (R^2=0.41, p<0.005) (E.IV). Nr. of patients n=8 (s-AD), n=4 (CU-AP); A number of 200-250 cored-, and 200-250 diffuse plaques for s-AD, and 200-250 diffuse plaques for CU-AP, were collected from 5 consecutive temporal cortical sections per patient; Scale bar: (A) 20µm; Errorbars (D): S.D.; Significance: *p<0.05; **p<0.005.

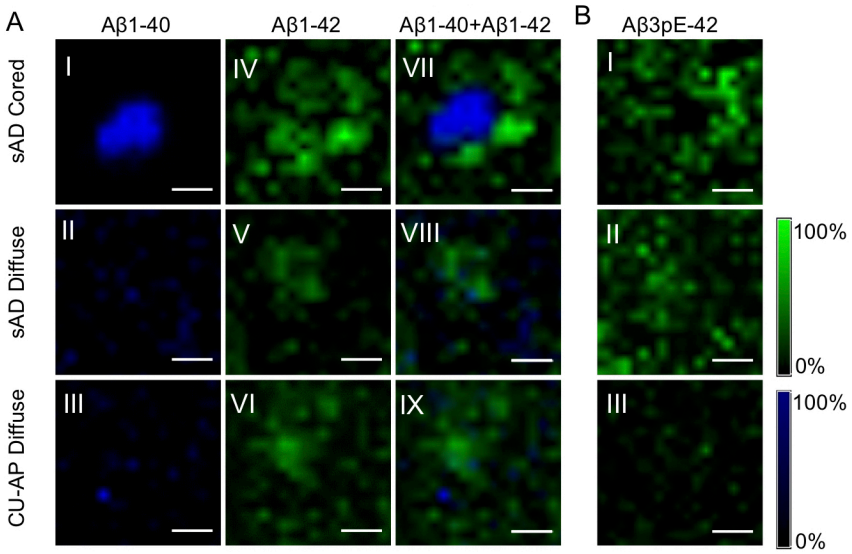

Figure 2. MALDI Imaging delineation of intraplaque Aβ **heterogeneity.** (A) MALDI Imaging MS: Single ion images of individual plaques from MALDI IMS analysis revealed a prominent localization of Aβ1-40 to the center of the cored plaques in s-AD (A.I), while the Aβ1-42 signal localized to the periphery of cored plaques in s-AD tissue (A.IV, see also image overlay, A.VII). Diffuse plaques in both s-AD (A.II, A.V) and CU-AP (A.III, A.VI) showed low Aβ1-40 signal, but a strong Aβ1-42 signal, that was homogenous across these plaques as highlighted in the overlay images (A.VIII, A.IX).
(B) MALDI IMS analysis did further reveal localization of AβpE3-42 to the periphery of cored plaques in s-AD (B.I) as well as diffuse plaques in s-AD (B.II), while only a very low signal was present for these peptides in the diffuse plaques in CU-AP (B.III).
MALDI IMS was performed on consecutive sections to the sections used for LCO imaging and LMPC. Nr. of patients n=8 (s-AD), n=4 (CU-AP); Scale bar: (A,B) 20µm. Intensity scales indicating maximum peak intensities of MALDI single ion signal

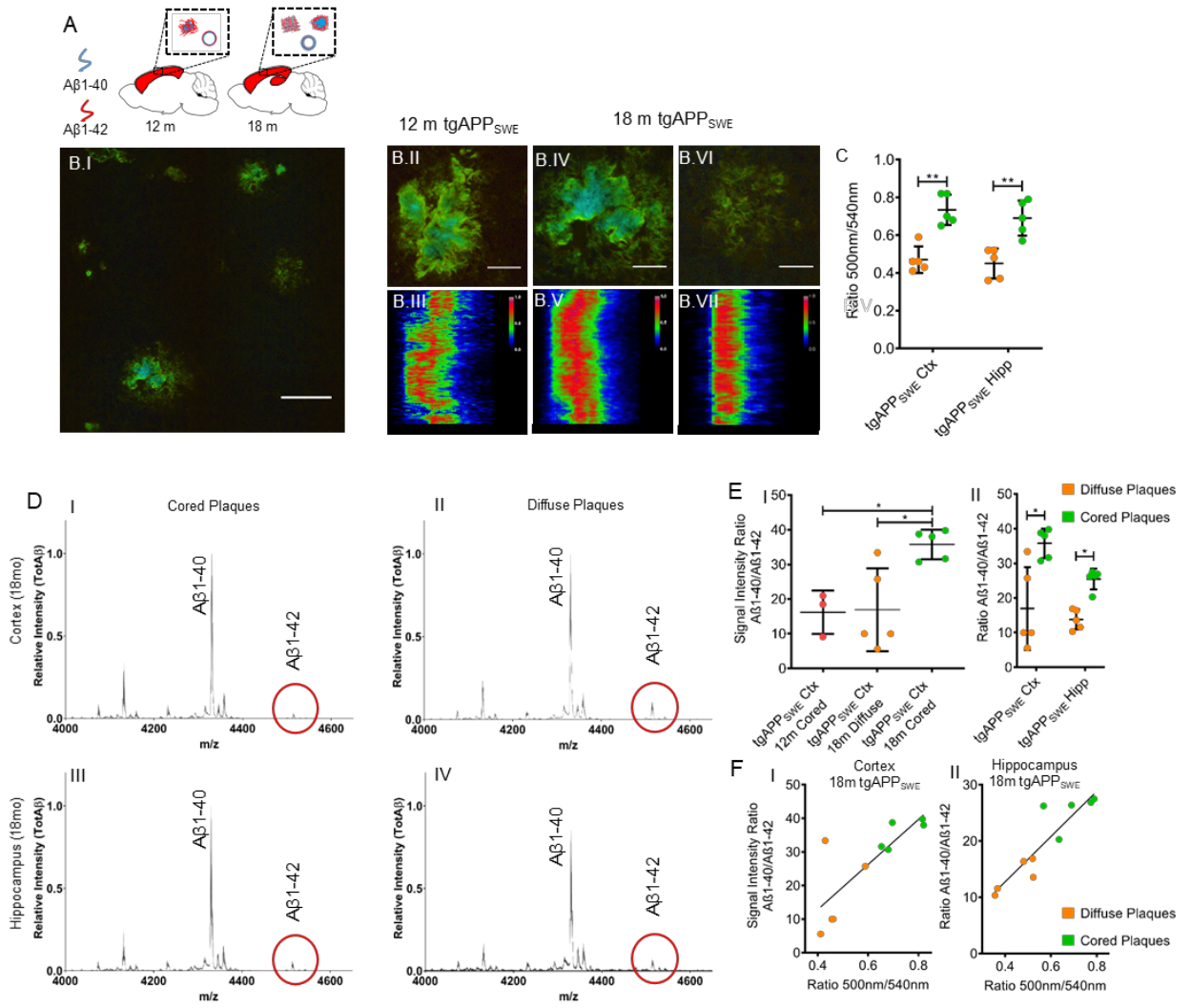

Figure 3. Aβ deposits in ageing tgAPP$_{SWE}$ mice. (A) Aβ plaque pathology, and vascular Aβ deposition was investigated in 12-month-old- (n=3) and 18-month-old-, male, tgAPP$_{SWE}$ mice (n=5) in cortex and hippocampus. (B.I) Widefield, hyperspectral fluorescence microscopy of cortex in 18-month-old tgAPP$_{SWE}$ mice show heterogenous plaque pathology. (B.II) Hyperspectral microscopy of cortical plaques in 12-month-old tgAPP$_{SWE}$ mice, shows small compact, plaques with presence of a core (B.II) as further reflected in an intermediate cross-sectional emission profile (B.III). LCO fluorescence imaging of cortical Aβ plaque pathology in 18-month-old tgAPP$_{SWE}$ mice, with zoom (B.IV) and cross-sectional emission profile of a cortical cored- (B.V) and diffuse- Aβ deposit (B.VI, VII). (C) Average 500nm/540nm ratio for distinct plaque subgroups, in two brain regions of 18-month-old mice reveal similar pattern between diffuse and cored deposits in both regions, resembling that of s-AD patients. Hyperspectrally classified plaques were then excised with laser microdissection and extracted with formic acid followed by immunoprecipitation and MALDI mass spectrometry (IP-MALDI MS). (D) Corresponding MALDI MS spectra of different plaque types show relative Aβ peptide intensities in cored (D.I,D.III) and diffuse (D.II, D.IV) plaques in the cortex (ctx, D.I, D.II) and hippocampus (hipp, D.III, D.IV) of 18 month old tgAPP$_{SWE}$ mice (n=5). Red circle highlight the Aβ1-42 peak, which is relatively higher in the diffuse deposits (D.II, D.IV) and that this trend is more prominent in cortical plaques (D.I, D.III).
(E) Statistical analysis reveal that small, cored plaques in 12-month-old tgAPP$_{SWE}$ mice display a similar Aβ1-40/Aβ1-42 ratio as diffuse plaques at 18 months. In contrast, the Aβ1-40/Aβ1-42 ratio was twofold higher in cored plaques in 18-month-old mice as compared to both diffuse plaque in 18-month-old mice and

small, cored plaques in 12-month-old mice (E.I). Similarly, for the 18-month-old animals, the Aβ1-40/Aβ1-42 signal ratio was consistently, two-fold increase in cored plaques as compared to diffuse plaques in the both cortex and hippocampus (E.II). Correlation of Aβ1-40/Aβ1-42 ratio with the 500nm/540nm emission ratio in cortex (F.I, R^2=0.64, p<0.005) and hippocampus (F.II, R^2=0.82, p<0.005). Nr. of animals n=5 (18-month-old), n=3 (12-month-old); A number of 15-20 cored, and 15-20 diffuse plaques, were collected from only cortex (12mo) and both, cortex and hippocampus (18mo), from 5 sagittal sections per animal. Scale bar: (B) 75µm, zoom: 20µm, Errorbars (C, E): S.D.; Significance: *p<0.05; **p<0.005.

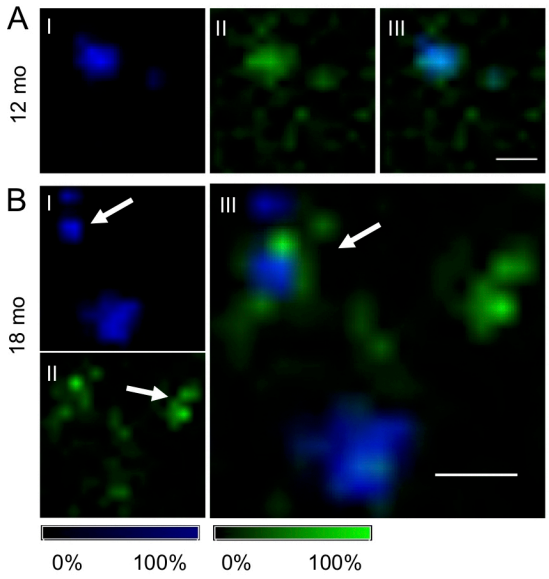

Figure 4. Aβ deposits in ageing tgAPP$_{SWE}$ mice. (A) For 12-month-old mice, MALDI imaging MS analysis revealed small compact plaques in with high levels of Aβ1-40 (A.I) and moderate localization of Aβ1-42 to the periphery (A.II), while still displaying high degree of (A.III) colocalization. (B) In 18-month-old tgAPP$_{SWE}$ mice, MALDI imaging MS reveals that Aβ1-40 pre-dominantly localizes to core structures of cored plaques (arrow, B.I). In contrast, Aβ1-42 localized primarily to diffuse plaques (arrow, B.II) and diffuse radial structures of cored deposits as seen in the overlay image (arrow, B.III). Nr. of animals n=5 (18-month-old), n=3 (12-month-old); MALDI IMS was performed on consecutive sections to the sections used for LCO imaging and LMPC. Scale bar: (A,B) 100µm; Intensity scales indicating maximum peak intensities of MALDI single ion signal

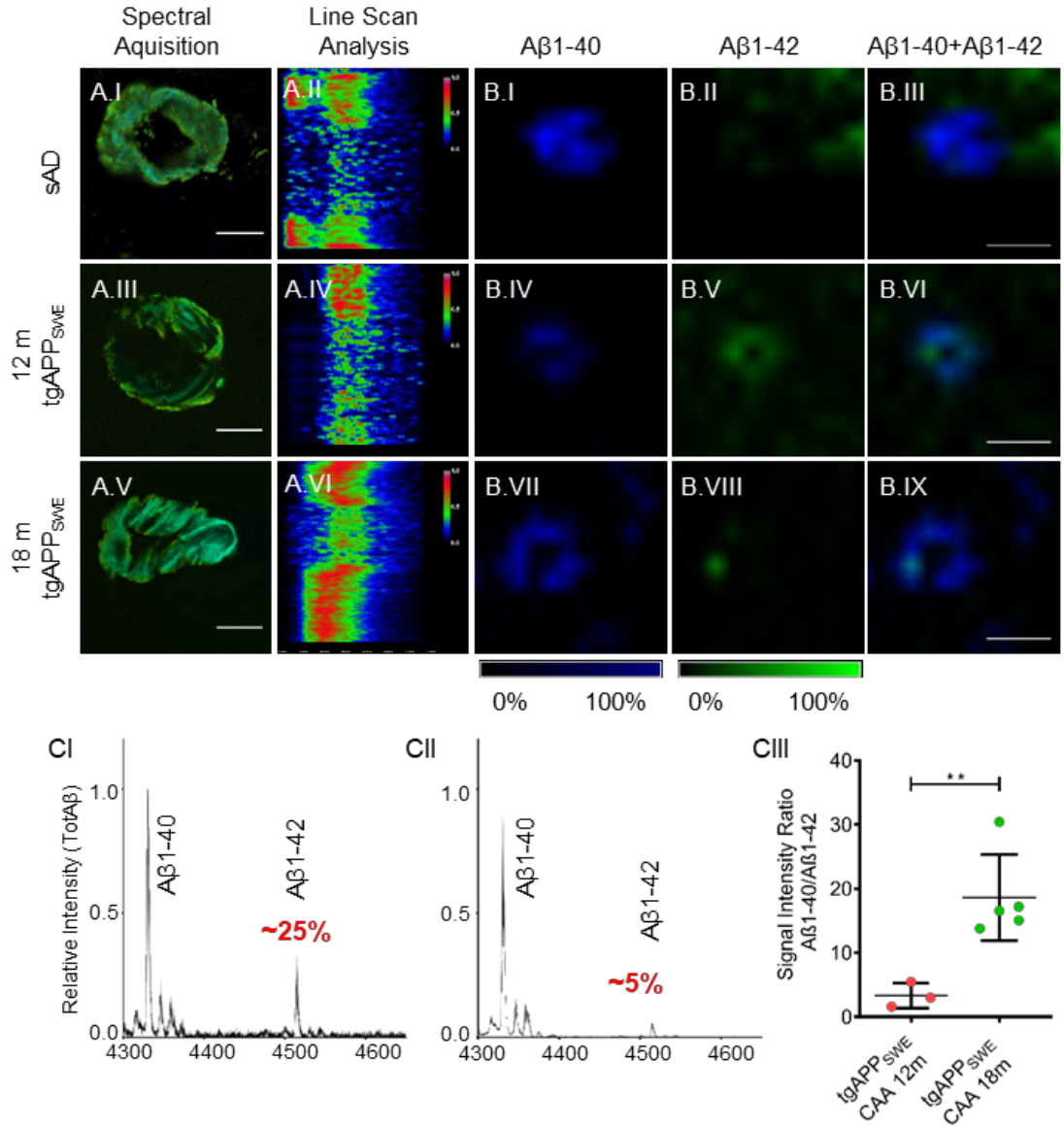

Figure 5. Parenchymal cerebral amyloid angiopathy (CAA) in s-AD patients and tgAPP$_{SWE}$ mice. Hyperspectral image and cross-sectional emission profile of CAA from s-AD tissue showed dominant q-FTAA emission (A.I,II). For 12-month-old (A.III,IV) and 18-month-old (A.V,VI) tgAPP$_{SWE}$ mice, an age dependent shift towards q-FTAA emission was observed. MALDI IMS showed a strong Aβ1-40 signal (B.I), with low Aβ1-42 levels (B.II, B.III). In younger tgAPP$_{SWE}$ mice MALD IMS verified that both Aβ1-40 (B.IV) and Aβ1-42 (B.V), are present, showing clear signal colocalization. In older mice, CAA consisted mainly of Aβ1-40 (B.VII), with a weak Aβ1-42 signal (B.VIII) with colocalization (B.IX). Nr. CAA per patient: ~50; Nr. of CAA per animal: 15-25; Scale bar: (A,B) 20µm
(C) Mass spectra of parenchymal CAA in (C.I) 12 month old (n=3) , and (C.II) 18 month old tgAPP$_{SWE}$ mice (n=5). The relative amount of Aβ1-42 in relation to the Aβ1-40 peptide differed significantly, and (C.III) comparative statistics of average ratios reveal a major increase in relative amounts of Aβ1-40 in older mice (18mo). A number of 15-25 CAA, were collected from 5 sagittal sections per animal. Errorbars (C.III): S.D.; Significance: **p<0.005.

Pyroglutamation of amyloid-βx-42 (Aβx-42) followed by Aβ1-40 deposition underlies plaque polymorphism in progressing Alzheimer's disease pathology

Wojciech Michno, Sofie Nyström, Patrick Wehrli, Tammaryn Lashley, Gunnar Brinkmalm, Laurent Guerard, Stina Syvänen, Dag Sehlin, Ibrahim Kaya, Dimitri Brinet, K. Peter R. Nilsson, Per Hammarström, Kaj Blennow, Henrik Zetterberg and Jörg Hanrieder

J. Biol. Chem. published online February 27, 2019

Access the most updated version of this article at doi: 10.1074/jbc.RA118.006604